

Orbital Decay and Evidence of Disk Formation in the X-ray Binary Pulsar OAO 1657-415

P. A. Jenke¹

MSFC/NPP, Huntsville, AL 35812, USA

M. H. Finger

Universities Space Research Association, Huntsville, AL 35805, USA

C. A. Wilson-Hodge

Marshall Space Flight Center, Huntsville, AL 35812, USA

and

A. Camero-Arranz

Universities Space Research Association, Huntsville, AL 35805, USA

Received _____; accepted _____

Not to appear in Nonlearned J., 45.

ABSTRACT

OA0 1657-415 is an eclipsing X-ray binary wind-fed pulsar that has exhibited smooth spin-up/spin-down episodes and has undergone several torque reversals throughout its long history of observation. We present a frequency history spanning nearly 19 years of observations from the Burst and Transient Source Experiment (CGRO/BATSE) and from the Gamma-Ray Burst Monitor (Fermi/GBM). The analysis suggests two modes of accretion: one resulting in steady spin-up during which we believe a stable accretion disk is present and one that results in what appears to be a random walk in spin frequency where an unstable accretion disk forms alternating in direction ("flip flop"). Orbital elements of the pulsar system are determined at several intervals throughout this history. With these ephemerides, statistically significant orbital decay ($\dot{P}/P = (-3.40 \pm 0.15) \times 10^{-6} \text{ yr}^{-1}$) is established suggesting a transition between wind-fed and disk-mediated accretion.

Subject headings: OA0 1657-415, Pulsar, X-ray Binary

1. Introduction

OA0 1657-415 is an accreting X-ray pulsar with a high mass companion. It was first detected by the Copernicus satellite in 1978 (Polidan et al. 1978). The companion is believed to be a Ofpe/WN9 supergiant (Mason et al. 2009). One of ten known eclipsing X-ray binary pulsars, the eclipse lasts 16% of the orbit or 1.7 days. OA0 1657-415’s moderate spin period (37 seconds) and its moderate orbital period (10.4 days) (Chakrabarty et al. 1993) gives it a unique placement on the Corbet diagram (Hulleman et al. 1998) which categorizes X-ray pulsars by spin period and orbital period. Due to the relatively short orbital period and spin period of this wind fed system it has been speculated that this system may be in transition from wind-fed to disk-mediated accretion (Mason et al. 2009). There is also considerable speculation that a transient accretion disk is formed from the companion’s stellar wind (Baykal 2000). This work, using data from the Burst and Transient Source Experiment (BATSE) previously on board the Compton Gamma-Ray Observatory (CGRO) and the Gamma-Ray Burst Monitor (GBM) on board Fermi, reveals orbital decay of OA0 1657-415 and provides evidence in favor of this evolution. By analyzing the torque vs. flux relationship, we also present evidence of a transient, but stable accretion disk.

2. Background

The different classes of high mass X-ray binaries (HMXB) can be plotted in a P_{spin} - P_{orb} diagram (Corbet 1986), or a Corbet diagram, where P_{spin} is the neutron star spin period and P_{orb} is the orbital period of the binary system (See Figure 1). The pink diamonds are Roche lobe filling high mass systems that have relatively short orbital periods and short spin periods. The wind fed systems (red asterisks) have longer orbital periods, avoiding Roche lobe filling, and longer spin periods due to weaker accretion torques. The Be systems (green circles) display correlation between orbital period and spin period, possibly due to

the longer orbital period system’s neutron star being further away from the donor star and thus sampling a weaker portion of the circumstellar disk (Waters and van Kerkwijk 1989). Other systems show anomalous behavior, such as SAX J2103.5+4545 (Camero Arranz et al. 2007) which is a Be/X-ray binary with a orbital period of 12.68 days and a pulse period of 358 seconds. This unusual orbital and pulse period for a Be/X-ray binary places it among the wind fed supergiants in the Corbet diagram. Another source that appears to defy these groups is OAO 1657-415. Its orbital period is 10.4 days and its pulse period is 37.1 seconds and occupies an intermediate region between sources with mass transfer via a stellar wind and Roche lobe overflow (Chakrabarty et al. 1993).

Identification of OAO 1657-415’s companion proved elusive for 15 years after its discovery (Kamata et al. 1990). In 1993, monitoring by CGRO/BATSE allowed sufficient data for the first orbital ephemeris to be calculated yielding a mass function for the system (Chakrabarty et al. 1993). Assuming the pulsar has a mass of $1.4 M_{\odot}$ and using the knowledge of the eclipse, Chakrabarty et al. (1993) calculated the mass of the companion to be $14 M_{\odot} \leq M_c \leq 18 M_{\odot}$ with a radius between 25 and 32 R_{\odot} . This yields a blue supergiant of stellar class B0-B6. Attempts to optically identify the companion failed due to a large column density but in 2002 a relatively bright star (2MASSJ17004888-4139214) was identified in the near-infrared that was coincident with a Chandra X-Ray Observatory position of OAO 1657-415 (Chakrabarty et al. 2002) and consistent with its companion’s spectral class. Due to the degeneracy of infrared color-color diagrams, infrared photometry did not provide decisive results. More detailed infrared spectroscopy performed in 2009 by Mason et al. (2009) concluded that OAO 1657-415’s companion is of a spectral type Ofpe/WN9 which is a transitional stage between a type OB and a Wolf-Rayet star characterized by high mass loss, low wind velocities, with exposed CNO-cycle products.

3. CGRO/BATSE Data

BATSE was an all-sky monitor designed to study gamma-ray bursts and transient source outbursts in the hard X-ray and soft gamma-ray bands (Fishman and et al. 1989). The observations reported here use data from the eight Large Area Detectors (LADs), which were 2025 cm² in area by 1.24 cm thick Na I(Tl) scintillators operated in the 20 keV-1.8 MeV band. These were located at the eight corners of the CGRO spacecraft. The LADs were uncollimated, with each detector viewing half of the sky. The pulse timing analyses uses the DISCLA channel 1 data, which consist of discriminator rates for the 20-50 keV band, continuously read out from all eight detectors with a resolution of 1.024 s. BATSE data used for the following analysis spans from 48362 to 50683 MJD (April 16, 1991 - August 23, 1997).

4. Fermi/GBM Data and preparation

GBM is an all sky monitor whose primary objective is to extend the energy range over which gamma-ray bursts are observed in the Large Area Telescope (LAT) on Fermi (Meegan et al. 2009). GBM consists of twelve NaI detectors with a diameter of 12.7 cm and a thickness of 1.27 cm and two BGO detectors with a diameter and length of 12.7 cm. The NaI detectors have an energy range from 8 keV to 1 MeV while the BGO's extend the energy range to 40 MeV. The current pulse timing analysis uses the first 3 channels of the CTIME data (8-12 keV, 12-25 keV, 25-50 keV) from the NaI detectors with a time resolution of 0.256 s. The daily light curves are visually inspected and times where the spacecraft is performing a rapid maneuver, SAA passages, gamma-ray bursts (GRBs) and contaminating features, such as solar events, that prevent a good background model fit are removed from the data. The data from channel 0-2 (corresponding to energies between 8 and 50 keV) are fit with an empirical background model which is subtracted from the data.

GBM data used for the following analysis spans from 54690 to 55824 MJD (August 12, 2008 - September 20, 2011).

5. Data Analysis

Because pulsars emit a large percentage of their radiation in periodic pulses, Fourier components of the source signal can be identified and extracted from the background. For details on this procedure see Camero-Arranz et al. (2010); Finger et al. (1999). In the case of BATSE data, short intervals (roughly 500 seconds) were fit to a Fourier expansion in pulse phase plus a quadratic spline model that accounts for the combined background and the average source flux. In the case of GBM data, short intervals (again roughly 500 seconds) of the residuals from the background subtraction were fit to a Fourier expansion in pulse phase. OAO 1657-415 pulse profiles were represented by six harmonics ($n = 6$) in this work. Additional harmonics did not resolve additional structure in the pulse profile. The Fourier expansion in pulse phase resulted in an estimated pulse profile (residual profile) for each data segment. For the purpose of creating a preliminary phase model the orbit was initially divided into 3 equally spaced intervals plus the occulted interval.

The times are barycentered using the JPL Planetary ephemeris DE200 (Standish 1990). Further time corrections are performed to remove the time delays from the orbital motion of the pulsar using a preliminary orbital model. This results in times that correspond to the pulsar emission time t^{em} and is computed from barycentered times (t^{bc}) by $t^{em} = t^{bc} - z$. The line of sight delay, z , associated with the binary orbit of the pulsar is given by Deeter et al. (1981)

$$z(t^{em}) = a_x \sin i [\sin \omega (\cos E - e) + (1 - e^2)^{\frac{1}{2}} \cos \omega \sin E] \quad (1)$$

where a_x is the projected semi-major axis of the pulsar’s orbit, i is the orbit’s inclination relative to the plane of the sky, ω is the periastron angle, and e is the orbital eccentricity. The eccentric anomaly, E , is related to time through Kepler’s equation,

$$E - e \sin E = \left(\frac{2\pi}{P_{orb}}\right)(t^{em} - \tau_p) \quad (2)$$

where P_{orb} is the orbital period and τ_p is the periastron epoch, the time at which the pulsar most closely approaches its companion. Initially, the orbital ephemeris from Bildsten et al. (1997) is used to correct the times for orbital motion. A preliminary phase model is estimated from historical trends in the frequency. The pulse phase model is a monotonically increasing function counting the number of pulses from the pulsar since a defined time τ referred to as the epoch. A simple phase model is:

$$\phi(t_k) = \phi_o + \nu_o(t_k - \tau) + \dot{\nu}_o \frac{(t_k - \tau)^2}{2} \quad (3)$$

where ν_o is the pulse frequency at time τ and ϕ_o is the phase at time τ . The pulse frequency, $\nu(t_k)$ is the first derivative of the phase model. In the simple case where $\dot{\nu}_o = 0$, $\nu(t_k) = \nu_o$, a constant frequency. As more knowledge is gained about the pulsar’s behavior, the phase model is refined by adding additional terms. The long term phase model is determined by fitting quadratic splines to the corrected phases.

Each unocculted interval was searched for a pulsed signal, in a narrow frequency band, using the Y_n statistic described in Finger et al. (1999). The search was performed on the first two harmonics and using channels 1+2 (12-50 keV) simultaneously for GBM and Channel 1 (20-50 keV) for BATSE data. The preliminary frequency history of OAO 1657-415 is shown in Figure 2 with a long term spin-up trend ($\dot{\nu} \sim 7.15 \times 10^{-8}$ Hz/day or $\dot{P} \sim -8.60 \times 10^{-6}$ day day $^{-1}$) being evident. Steady spin-up is evidence for a prograde accretion disk.

In order to calculate orbital elements, OAO 1657-415’s orbit was divided into 6 equally

spaced intervals plus the occulted interval. The residual profiles were folded for each of these intervals using the most recent ephemeris (Bildsten et al. (1997) and the best frequency from the above search). Although no frequency search was performed at this stage, the Y_2 was calculated for the previously determined frequency for GBM data. A template for the pulse profile was calculated by averaging the folded residual profiles over three orbits (18 folded profiles) of OAO 1657-415. For GBM data, the 12-25 keV energy band is used. Long term average pulse profiles from GBM data in three energy bands (8-12 keV, 12-25 keV, and 25-50 keV) are shown in figure 3. The morphology of the pulse changes from a relatively smooth single pulse at low energy to a double peaked asymmetric pulse with a fast rise and slow decay at higher energies. There is very little evolution of the pulse profile with luminosity or time. The 12-25 keV pulse profile is representative of the template profiles used. The template profile was normalized and fit to the folded profiles along with a phase model. A scaling factor and phase offset is calculated from the fit. For BATSE data, phase offsets that could unambiguously determine the phase to 3σ were selected (i.e. phase offsets error ≤ 0.15). For GBM data, a cut in Y_2 (≥ 8) was used to select good intervals. The phase model is then corrected for the fitted phase offsets to produce corrected phases.

The corrected phases and barycentered times were fit to an orbital model plus a polynomial (see figure 4). The first term of the polynomial is the linear trend in time expected from the phases while the second term represents the frequency change of the source over the interval. Higher order terms account for torque noise inherent in these systems.

6. Timing Results

Intervals where pulsations were clearly detected and where the phases did not deviate radically from the phase model (minimal torque noise) were chosen from BATSE and GBM

data. Orbital fits to this data were performed for three orbit intervals from the selected data. Appendix A shows the intervals and results of each fit. A new orbital ephemeris was determined by averaging the orbital elements from each fit (See Table 1). All the orbital epochs are plotted against time with a linear trend removed (See Figure 5). A quadratic fit in orbit number from all the determined epochs reveals the long term orbital trend in the orbit of OAO 1657-415. The Chakrabarty et al. (1993) epoch is excluded in this calculation because the data they used overlaps the data used here. Nevertheless, the Chakrabarty et al. (1993) epoch is consistent with these results.

Using the expansion of the epoch, the derivative of the orbital period is determined from the quadratic fit:

$$T_{\pi/2} = T_o + nP_{orbit} + \frac{1}{2}n^2P_{orbit}\dot{P}_{orbit} \quad (4)$$

The inclusion of the epoch calculated from INTEGRAL data by Barnstedt et al. (2008) was rejected on the basis that it significantly reduces the quality of the quadratic fit ($\Delta\chi^2 > 20,000$) in Figure 5. This suggests that the error in the Barnstedt et al. (2008) epoch is significantly underestimated.

7. Torque-Flux Correlation Results

We compare our measured frequency rate ($\dot{\nu}$) with Swift/BAT fluxes (Figure 6). In order to determine a calibration for the BAT rates, observations (~ 36 ksec) of OAO 1657-415 by *RXTE* were obtained on August 11, 2011. The *RXTE*/PCU2 (5–50 keV) spectra were fitted in XSPEC 12.7¹ with a model which includes a low-energy absorption,

¹Goddard Space Flight Center. Arnaud K.A, Dorman B, Gordon C, HEASARC Software Development

a few gaussian lines, a power law and the local model fdcut (Tanaka 1986), in XSPEC notation $\text{phabs} \times (\sum \text{gaussian} + \text{powerlaw}) \times \text{fdcut}$. The energy flux from 5-50 keV during these observations is $4.15 \times 10^{-9} \text{ ergs cm}^{-2} \text{ s}^{-1}$. Comparing this energy flux and the rates from the Swift/BAT² transient monitor (15-50 keV) for approximately the same times, a conversion factor of $9.5133 \times 10^{-8} \text{ ergs counts}^{-1}$ was determined. Rates from observations of OAO 1657-415 by the Swift/BAT transient monitor were folded on OAO 1657-415's orbital period and converted to fluxes using the above conversion factor. The maximum flux during an orbital cycle was chosen as a proxy for the intrinsic flux of the source. This is because the orbital flux profiles suggests OAO 1657-415 is partially obscured during much of its orbit. This is consistent with locally large column densities inferred for the source (Naik et al. 2009; Audley et al. 2006). The maximum of the folded fluxes during the intervals in which the derivative of the frequency was determined is plotted against the frequency derivative and is shown in figure 6. The intervals where the frequencies were not monotonically increasing or decreasing were rejected to insure accurate determination of the frequency derivative. The intervals were at least 12 days to ensure the maximum flux during an orbital period could be determined. Figure 6 shows a strong flux- $\dot{\nu}$ correlation when $\dot{\nu}$ is greater than $3 \times 10^{-12} \text{ Hz s}^{-1}$.

8. Discussion

Orbital decay provides evidence that the system is evolving toward Roche lobe over-flow. Theoretically it is possible to constrain orbital decay (assuming the inclination of the orbit is constant) by calculating $\dot{\omega}/\omega$ and \dot{a}_x/a_x where a_x is the semi-major axis. The error in the orbital ephemerides and considerable torque noise in the system exclude

²<http://heasarc.gsfc.nasa.gov/docs/swift/results/transients/>

a useful constraint on orbital decay by this method but are consistent with what was measured from the epoch residuals.

A strong stellar wind will transfer angular momentum from the system to a halo surrounding the binary system which will lead to orbital decay. Following Shore et al. (1992), the system may be viewed as a massive star losing material, via stellar wind, to a ring beyond the L_2 point of the system. If a is the semimajor axis of the orbit then a_ϵ is the radius of the ring of escaping material. In this case $a_\epsilon > 1.2a$. The ratio of escaping angular momentum per unit mass to total angular momentum per unit mass is:

$$\gamma = \frac{(M_c + M_p)^2}{M_c M_p} \left(\frac{a_\epsilon}{a(1 - e^2)} \right)^{\frac{1}{2}}, \quad (5)$$

where M_c is the mass of the companion, M_p is the mass of the neutron star, e is the eccentricity of the orbit. Using $M_p = 1.4M_\odot$, assuming $\dot{M}_c \gg \dot{M}_p$, using previous results for e and noting that $a \geq a_x \sin i$, the predicted orbital decay from mass loss through a stellar wind assuming values for \dot{M} consistent with fluxes in Figure 6 is:

$$-\frac{\dot{P}_{orb}}{P_{orb}} = -(1 + 3\gamma) \frac{\dot{M}_c}{M_c + M_p} + 3 \frac{\dot{M}_c}{M_c}, \quad (6)$$

$$-\frac{\dot{P}_{orb}}{P_{orb}} > 1.45 \times 10^{-6} \text{yr}^{-1}, \quad (7)$$

where P_{orb} is the period of the orbit. Although spin-orbit quadrupole coupling (Lai et al. 1995) almost assuredly plays a role in orbital decay, the predicted orbital decay from stellar wind mass loss is sufficient to explain the measured orbital decay in OAO 1657-415.

Utilizing values for the Roche lobe radius (R_L) and the masses of the neutron star and companion from Mason et al. (2011), OAO 1657-415 will have a common envelope with its companion in 8 to 17 10^4 years. This is contingent on the companion maintaining its current evolutionary status for that length of time. If OAO 1657-415's companion is experiencing the onset of a Wolf-Rayet stage then it is probable that OAO 1657-415 will evolve into a common envelope with a Wolf-Rayet star given that the Wolf-Rayet phase lasts 3 to 5 10^5

years (Prantzos et al. 1986).

Flux-torque correlations are expected when an accretion disk is present. To test for the existence of an accretion disk assuming a high \dot{M} , the correlated part of the data where $\dot{\nu} > 3 \times 10^{-12} \text{ Hz s}^{-1}$ is fit to a model of disk accretion, $\dot{\nu} \propto F^{\frac{6}{7}}$ (Rappaport and Joss 1977), and is shown in Figure 6. Using this model, the resultant fit, and a range of values for the other parameters, a distance to the OAO 1657-415 can be calculated. Using a disk accretion model, the distance to the OAO 1657-415 can be calculated and is consistent with what is found in the literature. From Ghosh and Lamb (1979), the neutron star spin derivative, $\dot{\nu}$, may be calculated in terms of the moment of inertia, I , mass of the neutron star, M_p , mass accretion rate, \dot{M}_p , the radius of the inner point of the Keplerian disk, r_o , and a function, which is of order unity, that depends only on the fastness parameter, $n(\omega_s)$:

$$\dot{\nu} = n(\omega_o)(2\pi I)^{-1}(GM_p r_o)^{1/2} \dot{M}_p, \quad (8)$$

where G is the gravitational constant. Following Wang (1996) the inner point of the Keplerian disk is given by:

$$r_o = k(2GM)^{-1/7} \mu^{4/7} \dot{M}_p^{-2/7}, \quad (9)$$

where μ is the magnetic dipole moment and k is such that $r_o = k r_a$ where r_a is the Alfvén radius for spherical accretion. Assuming at least partial threading of the accretion disk by the magnetosphere, k is less than unity. Assuming a dipole magnetic field and that the gravitational energy of the accreted material is converted to X-rays i.e. $F = \alpha \frac{GM}{R_n} \frac{\dot{M}}{4\pi d^2}$ then,

$$\begin{aligned} \dot{\nu} = & 2.46 \times 10^{-6} (n(\omega_o) k)^{1/2} \alpha^{-6/7} \left(\frac{M}{M_\odot} \right)^{-3/7} \\ & \times \left(\frac{I}{I_{45}} \right)^{-1} \left(\frac{R_n}{R_6} \right)^{12/7} \left(\frac{B_n}{B_{12}} \right)^{2/7} d^{12/7} F^{6/7} \end{aligned} \quad (10)$$

where α is the bolometric fraction, R_n is the neutron star radius, d is the distance to the neutron star in kiloparsecs, and B is the magnetic field of the neutron star. By choosing a modest range of possible neutron star masses, $1 \leq M_n \leq 1.8$, models of the equation of state of neutron stars determine M , R and I . From figure 7, this range of neutron star masses results in $0.5 \leq (M/M_\odot)^{-3/7} R_6^{12/7} I_{45}^{-1} \leq 1.6$ (Wiringa et al. 1988; Arnett and Bowers 1977; Pandharipande et al. 1976). The model of the energy spectrum was used to infer the bolometric fraction of the luminosity from 5 - 50 keV. For OAO 1657-415 it was determined that $0.5 \leq \alpha \leq 0.8$. Although a cyclotron resonance scattering feature (cyclotron line) has never been detected for OAO 1657-415, the energy of the cyclotron lines in other X-ray binaries range between 10 - 60 keV. Broadening this range to 10 - 100 keV implies a magnetic field strength range for this population to be $1.0 \leq B_{12} \leq 10.0$ Gauss. The factor, $(n(\omega_o)k)^{1/2}$, is assumed for this work, to be between 0.8 and 1.0. Using the fitted results in figure 6 and the above relation for an accretion disk, Equation 10, the distance to OAO 1657-415 can be constrained to between 3 and 16 kpc which is consistent with Mason et al. (2009), $4.4 \leq d \leq 12$ kpc. The existence of a long lived (days to months) transient accretion disk is consistent with the flux- $\dot{\nu}$ correlation and the distance to the star.

A question of considerable importance to these type of systems is how a stellar wind can transfer nearly uniform (averaged over a few days) torque to the neutron star for periods of months especially considering the complex environment of the neutron star. Even considering a stable wind emanating from the companion which is unlikely (Naik et al. 2009), the disrupting presence of a neutron star and its accompanying X-rays irradiating the wind and the companion will add considerable complexity to the system. Aside from the short term periods of spin-up and spin-down, the long term decrease in spin period that has occurred since the discovery of the source suggests that the torque on the neutron star does not stem from stochastic processes. Figure 6 suggests unstable prograde and retrograde transient (hours) accretion disks, described by Taam and Fryxell (1989), form

around OAO 1657-415 contributing to the torque responsible for $\dot{\nu} = \pm 3 \times 10^{-12}$ Hz/s. An occasional longer (days) stable prograde accretion disk accounts for the torques responsible for $\dot{\nu} > 3 \times 10^{-12}$ hz/s. This may shift the balance from a purely stochastic spin history to one in which an overall spin-up is observed.

The correlated part of figure 6 ($\dot{\nu} > 3 \times 10^{-12}$ hz/s) spans the same flux range as the uncorrelated part. If flux is a proxy for \dot{M} then the formation of the stable prograde accretion disk is not triggered by high \dot{M} but must have some other, unknown, triggering mechanism. Additional 3-D hydrodynamic simulations are needed to understand these new observations. Traditionally, the term wind-fed X-ray binaries has implied Bondi-Hoyle-Lyttleton accretion while disk-fed systems imply Roche-lobe overflow. Observations of accreting X-ray binaries are beginning to depict a much more complicated picture with systems that seem to lie in between the wind-fed and Roche-lobe overflow groups.

Acknowledgements

I would like to acknowledge Slawomir Suchy for the use of his results from his observations of OAO 1657-415 by *RXTE*. M. F. and A. C. acknowledge support from NASA grants NNX08AW06G and NNX11AE24G. This research was supported by an appointment to the NASA Postdoctoral Program at the Marshall Space Flight Center, administered by Oak Ridge Associated Universities through a contract with NASA.

A. Results from orbital fits

REFERENCES

- Arnett, W. D. and Bowers, R. L.: 1977, *ApJS* **33**, 415
- Audley, M. D., Nagase, F., Mitsuda, K., Angelini, L., and Kelley, R. L.: 2006, *MNRAS* **367**, 1147
- Barnstedt, J., Staubert, R., Santangelo, A., Ferrigno, C., Horns, D., Klochkov, D., Kretschmar, P., Kreykenbohm, I., Segreto, A., and Wilms, J.: 2008, *A&A* **486**, 293
- Baykal, A.: 2000, *MNRAS* **313**, 637
- Bildsten, L., Chakrabarty, D., Chiu, J., Finger, M. H., Koh, D. T., Nelson, R. W., Prince, T. A., Rubin, B. C., Scott, D. M., Stollberg, M., Vaughan, B. A., Wilson, C. A., and Wilson, R. B.: 1997, *ApJ* **113**, 367
- Camero-Arranz, A. et al.: 2010, *ApJ* **708**, 1500
- Camero Arranz, A., Wilson, C. A., Finger, M. H., and Reglero, V.: 2007, *A&A* **473**, 551
- Chakrabarty, D. et al.: 1993, *ApJ* **403**, L33
- Chakrabarty, D. et al.: 2002, *ApJ* **573**, 789
- Corbet, R. H. D.: 1986, *MNRAS* **220**, 1047
- Deeter, J. E., Boynton, P. E., and Pravdo, S. H.: 1981, *ApJ* **247**, 1003
- Finger, M. H. et al.: 1999, *ApJ* **517**, 449
- Fishman, G. J. and et al.: 1989, *Proc. Gamma-Ray Observatory Science Workshop*, ed. W. N. Johnson (Greenbelt, MD: NASA GSFC)
- Ghosh, P. and Lamb, F. K.: 1979, *ApJ* **234**, 296

- Hulleman, F., in 't Zand, J. J. M., and Heise, J.: 1998, *A&A* **337**, L25
- Kamata, Y., Koyama, K., Tawara, Y., Makishima, K., Ohashi, T., Kawai, N., and Hatsukade, I.: 1990, *PASJ* **42**, 785
- Lai, D., Bildsten, L., and Kaspi, V. M.: 1995, *ApJ* **452**, 819
- Mason, A. B., Clark, J. S., Norton, A. J., Crowther, P. A., Tauris, T. M., Langer, N., Negueruela, I., and Roche, P.: 2011, *ArXiv e-prints*
- Mason, A. B., Clark, J. S., Norton, A. J., Negueruela, I., and Roche, P.: 2009, *A&A* pp 281–286
- Meegan, C., Lichti, G., Bhat, P. N., Bissaldi, E., Briggs, M. S., Connaughton, V., Diehl, R., Fishman, G., Greiner, J., Hoover, A. S., van der Horst, A. J., von Kienlin, A., Kippen, R. M., Kouveliotou, C., McBreen, S., Paciesas, W. S., Preece, R., Steinle, H., Wallace, M. S., Wilson, R. B., and Wilson-Hodge, C.: 2009, *ApJ* **702**, 791
- Naik, S., Mukherjee, U., Paul, B., and Choi, C. S.: 2009, *Advances in Space Research* **43**, 900
- Pandharipande, V. R., Pines, D., and Smith, R. A.: 1976, *ApJ* **208**, 550
- Polidan, R. S., Pollard, G. S. G., Sanford, P. W., and Locke, M. C.: 1978, *Nature* **275**, 296
- Prantzos, N., Doom, C., De Loore, C., and Arnould, M.: 1986, *ApJ* **304**, 695
- Rappaport, S. and Joss, P. C.: 1977, *Nature* **266**, 683
- Shore, S. N., Livio, M., and Heuvel, E. P. J.: 1992, *Interacting Binaries*, Springer-Verlag
- Standish, Jr., E. M.: 1990, *A&A* **233**, 252
- Taam, R. E. and Fryxell, B. A.: 1989, *ApJ* **339**, 297

Tanaka, Y.: 1986, in D. Mihalas & K.-H. A. Winkler (ed.), *IAU Colloq. 89: Radiation Hydrodynamics in Stars and Compact Objects*, Vol. 255 of *Lecture Notes in Physics*, Berlin Springer Verlag, p. 198

Wang, Y.-M.: 1996, *ApJ* **465**, L111+

Waters, L. B. F. M. and van Kerkwijk, M. H.: 1989, *A&A* **223**, 196

Wiringa, R. B., Fiks, V., and Fabrocini, A.: 1988, *Phys. Rev. C* **38**, 1010

This manuscript was prepared with the AAS L^AT_EX macros v5.2.

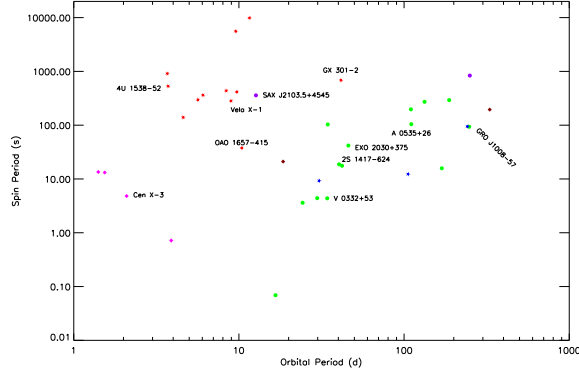


Fig. 1.— This figure shows high mass X-ray binaries plotted on a Corbet diagram. The red asterisk are the wind fed supergiants while the pink diamonds are the Roche-Lobe Overflow supergiants. OAO 1657-415 (labeled) has a position that suggests it is transitioning between the two. The green and purple circles are the transient and persistent Be/X-ray binaries respectfully while the blue stars are the likely Be X-ray binaries. The brown diamond is a Supergiant Fast X-ray Transient (SFXT).

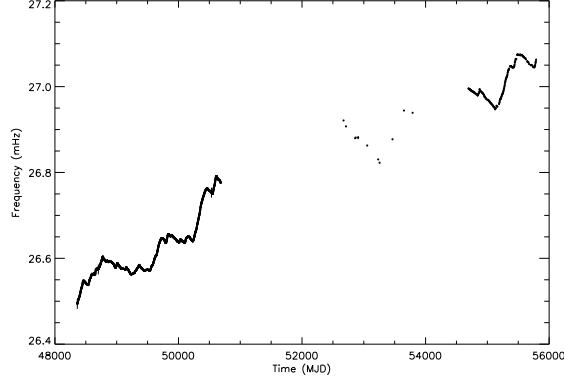


Fig. 2.— The frequency history of OAO 1657-415 extracted from BATSE data (left), INTEGRAL data from Barnstedt et al. (2008) (center), and GBM data (right).

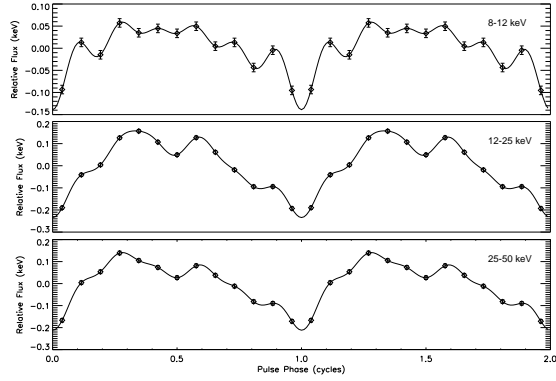


Fig. 3.— Average pulse profiles extracted from GBM data for ten orbits of OAO 1657-415 for 8-12 keV (top panel), 12-25 keV (middle panel), and 25-50 keV (bottom panel). Two cycles are shown for clarity.

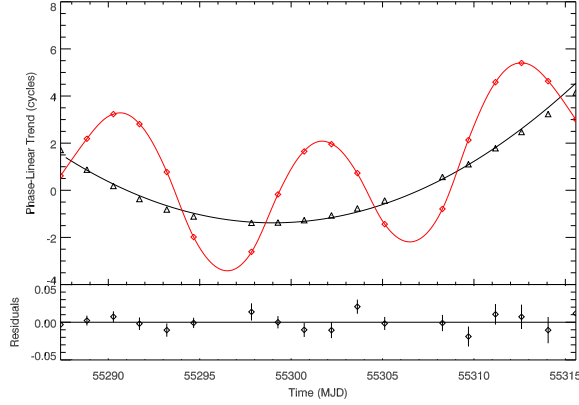


Fig. 4.— The black curve is the pulse phase model minus a linear trend in emission time for one 3 orbit fit. The black triangles are the measured phases using times corrected for the estimated orbit with the same linear trend in barycentered time removed. The red diamonds are the same phases with the same linear trend removed using times not orbitally corrected. The red curve is the best fit model of the phases with the same linear trend removed. The lower panel displays the residual to the fit of the orbital model.

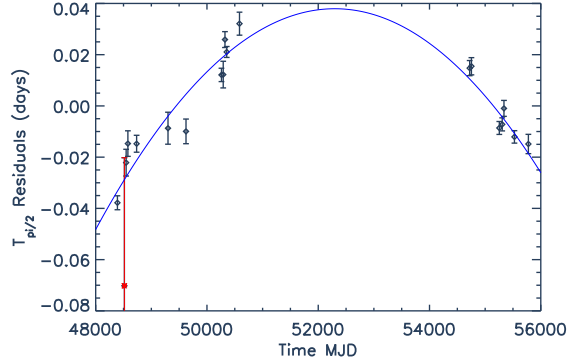


Fig. 5.— Diamonds are orbital epochs for each ephemerides with a linear trend removed. The line is a quadratic fit to the epochs. The epochs to the left are calculated from BATSE data while the epochs on the right are calculated from GBM data. The epoch calculated by Chakrabarty et al. (1993) is labeled as a red star and is excluded in the quadratic fit.

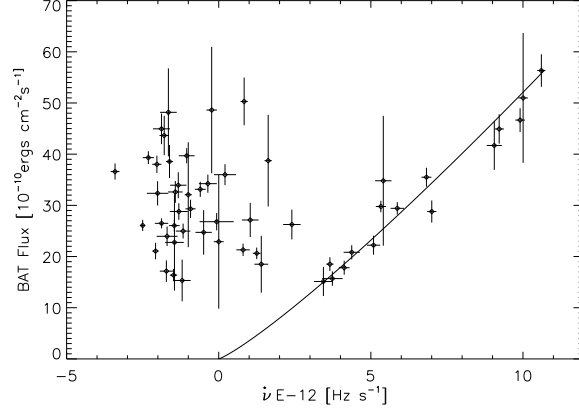


Fig. 6.— Swift/BAT flux versus the spin-up of OAO 1657-415 measured using GBM data. The curve is a model ($\dot{\nu} \propto F^{6/7}$) that is fit to the data where spin-up greater than 3×10^{-12} Hz/s.

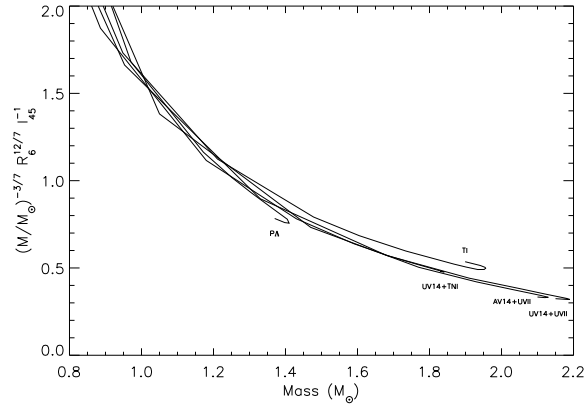


Fig. 7.— Models of the mass of a neutron star in terms of $(M/M_{\odot})^{-3/7} R_6^{12/7} I_{45}^{-1}$ (Wiringa et al. 1988; Arnett and Bowers 1977; Pandharipande et al. 1976). The type of model is insensitive to this grouping of parameters.

Table 1: Average Orbital Elements for OAO 1657-415.

Epoch	T_o	55776.99578(75) MJD
Orbital Period	P_{orb}	10.446953(15) days
Orbital Decay	\dot{P}_{orb}	$(-9.74 \pm 0.42) \times 10^{-8}$
Proj. Semimajor axis	$a_x \sin i$	106.157 ± 0.083 lt-sec
Long. of Periastron	ω	$92.69^\circ \pm 0.67^\circ$
Eccentricity	e	0.1075 ± 0.0012
Pulsar Mass Function	$f_x(M)$	11.473 ± 0.027 M_\odot

Table 2: Orbital Ephemerides for OAO 1657-415.

Start MJD	$T_{\pi/2}^a$ [MJD]	$a_x \sin i^a$ [lt-sec]	$e \cos \omega$	$e \sin \omega$	χ^2	DOF
48370.7	48390.6549 \pm 0.0027	106.49 \pm 0.29	-0.0053 \pm 0.0026	0.1151 \pm 0.0038	9.8	8
48527.5	48547.3800 \pm 0.0052	104.01 \pm 0.61	-0.0071 \pm 0.0027	0.1120 \pm 0.0046	23.9	8
48558.8	48578.7293 \pm 0.0050	106.05 \pm 0.47	-0.0011 \pm 0.0032	0.1047 \pm 0.0050	14.8	8
48715.5	48735.4386 \pm 0.0033	106.34 \pm 0.35	-0.0032 \pm 0.0035	0.1124 \pm 0.0057	7.6	8
49279.7	49299.5984 \pm 0.0062	105.09 \pm 0.60	-0.0069 \pm 0.0037	0.0999 \pm 0.0052	23.8	8
49603.6	49623.4633 \pm 0.0048	106.42 \pm 0.52	-0.0096 \pm 0.0034	0.1101 \pm 0.0052	18.7	8
50240.9	50260.7701 \pm 0.0026	106.16 \pm 0.29	-0.0053 \pm 0.0022	0.1061 \pm 0.0032	12.3	8
50272.2	50292.1121 \pm 0.0052	106.82 \pm 0.56	-0.0098 \pm 0.0036	0.1140 \pm 0.0056	21.5	8
50303.5	50323.4677 \pm 0.0031	106.90 \pm 0.34	0.0061 \pm 0.0032	0.1071 \pm 0.0048	1.5	8
50334.9	50354.8047 \pm 0.0021	105.40 \pm 0.23	-0.0042 \pm 0.0021	0.1047 \pm 0.0032	6.8	8
50564.7	50584.6562 \pm 0.0045	107.08 \pm 0.51	-0.0035 \pm 0.0031	0.1162 \pm 0.0050	16.4	8
54700.0	54721.7666 \pm 0.0030	106.30 \pm 0.30	-0.0033 \pm 0.0027	0.1045 \pm 0.0048	3.4	8
54732.0	54753.1092 \pm 0.0034	105.74 \pm 0.36	-0.0086 \pm 0.0031	0.1018 \pm 0.0044	12.2	9
55243.0	55254.5552 \pm 0.0025	105.84 \pm 0.30	-0.0113 \pm 0.0024	0.1015 \pm 0.0036	14.4	9
55286.0	55306.7930 \pm 0.0025	106.31 \pm 0.28	-0.0056 \pm 0.0022	0.1021 \pm 0.0036	14.8	9
55317.0	55338.1411 \pm 0.0031	107.00 \pm 0.44	-0.0055 \pm 0.0024	0.1114 \pm 0.0038	23.0	9
55505.0	55526.1813 \pm 0.0024	106.36 \pm 0.28	0.0010 \pm 0.0025	0.1098 \pm 0.0040	8.4	9
55765.0	55776.9135 \pm 0.0038	106.52 \pm 0.53	-0.0064 \pm 0.0024	0.1071 \pm 0.0036	26.5	6

^aErrors are statistical and inflated to reflect χ^2 .